*Inorg. Chem.* **2008**, *47*, 7792−7801


# Unravelling the Intrinsic Features of NO Binding to Iron(II)- and Iron(III)-Hemes

**Barbara Chiavarino,[†] Maria Elisa Crestoni,[†] Simonetta Fornarini,*[,†] and Carme Rovira*[,‡]**

*Dipartimento di Chimica e Tecnologia del Farmaco, Università di Roma "La Sapienza", P.le A. Moro 5, I-00185 Roma, Italy, Laboratori de Simulació Computacional i Modelització (CoSMoLab), Parc Científic de Barcelona, Josep Samitier 1−5, 08028 Barcelona, Spain, and Institut de Química Teòrica i Computacional (IQTCUB) and Institució Catalana de Recerca i Estudis Avançats (ICREA), Passeig Lluís Companys 23, 08018 Barcelona, Spain*

Received May 26, 2008

Electrospray ionization of appropriate precursors is used to deliver $[Fe^{III}\text{-heme}]^+$ and $[Fe^{II}\text{-hemeH}]^+$ ions as naked species in the gas phase where their ion chemistry has been examined by Fourier transform ion cyclotron resonance (FT-ICR) mass spectrometry. In the naked, four-coordinate $[Fe^{II}\text{-hemeH}]^+$ and $[Fe^{III}\text{-heme}]^+$ ions, the intrinsic reactivity of iron(II)- and iron(III)-hemes is revealed free from any influence due to axial ligand, counterion, or solvent effects. Ligand (L) addition and ligand transfer equilibria with a series of selected neutrals are attained when $[Fe^{II}\text{-hemeH}]^+$, corresponding to protonated $Fe^{II}$-heme, is allowed to react in the FT-ICR cell. A Heme Cation Basicity (HCB) ladder for the various ligands toward $[Fe^{II}\text{-hemeH}]^+$, corresponding to $-\Delta G^\circ$ for the process $[Fe^{II}\text{-hemeH}]^+ + L \rightarrow [Fe^{II}\text{-hemeH(L)}]^+$ and named $HCB^{II}$, can thus be established. The so-obtained $HCB^{II}$ values are compared with the corresponding $HCB^{III}$ values for $[Fe^{III}\text{-heme}]^+$. In spite of pronounced differences displayed by various ligands, NO shows a quite similar HCB of about 67 kJ $mol^{-1}$ at 300 K toward both ions, estimated to correspond to a binding energy of 124 kJ $mol^{-1}$. Density Functional Theory (DFT) computations confirm the experimental results, yielding very similar values of NO binding energies to $[Fe^{II}\text{-hemeH}]^+$ and $[Fe^{III}\text{-heme}]^+$, equal to 140 and 144 kJ $mol^{-1}$, respectively. The kinetic study of the NO association reaction supports the equilibrium HCB data and reveals that the two species share very close rate constant values both for the forward and for the reverse reaction. These gas phase results diverge markedly from the kinetics and thermodynamic behavior of NO binding to iron(II)- and iron(III)-heme proteins and model complexes in solution. The requisite of either a very labile or a vacant coordination site on iron for a facile addition of NO to occur, suggested to explain the bias for typically five-coordinate iron(II) species in solution, is fully supported by the present work.

## Introduction

Nitric oxide (NO) is known to play a fundamental role in a variety of biochemical processes and physiological activities such as blood pressure regulation, neurotransmission, and immune response.[1] The primary interaction for NO under bioregulatory conditions is directed to metal centers, notably the heme group of heme proteins, including soluble guanylyl cyclase, myoglobin, cytochrome P450, catalase, and peroxidase enzymes.[2] A heme center is also involved in the in vivo generation of NO by oxidation of arginine catalyzed by nitric oxide synthase proteins.[3] In this context, considerable efforts have been devoted to elucidate mechanistic aspects of solution phase reactions of NO with iron porphyrins and

* To whom correspondence should be addressed. E-mail: simonetta.fornarini@uniroma1.it.
† Università di Roma "La Sapienza".
‡ CoSMoLab, IQTCUB, ICREA.

(1) (a) McCleverty, J. A. *Chem. Rev.* **2004**, *104*, 403. (b) Murad, F. *Angew. Chem., Int. Ed.* **1999**, *38*, 1856. (c) *Nitric Oxide Chemistry*; Richter-Addo, G. B., Legzdins, P., Burstyn, J., Eds.; *Chem. Rev.* **2002**, *102* (4), 857.

(2) (a) Zhao, Y.; Brandish, P. E.; Ballou, D. P.; Marletta, M. A. *Proc. Natl. Acad. Sci. U.S.A.* **1999**, *96*, 14753. (b) Brunori, M. *Trends Biochem. Sci.* **2001**, *26*, 209. (c) Shimizu, H.; Obayashi, E.; Gomi, Y.; Arakawa, H.; Park, S.-Y.; Nakamura, H.; Adachi, S.-I.; Shoun, H.; Shiro, Y. *J. Biol. Chem.* **2000**, *275*, 4816. (d) Franke, A.; Stochel, G.; Jung, C.; Van Eldik, R. *J. Am. Chem. Soc.* **2004**, *126*, 4181. (e) Munro, A. W.; McLean, K. J.; Girvan, H. M. Ubiquitous Roles of Cytochrome P450 Proteins. In *Metal Ions in Life Sciences*; Sigel, A., Sigel, H., Sigel, R. K. O., Eds.; Wiley: New York, 2007; Vol. *3*, p 285.


10.1021/ic800953w CCC: $40.75

Published on Web 08/06/2008

heme proteins. In particular, because several facets of the biochemical role of NO are governed by metal-nitrosyl bond formation and rupture, systematic mechanistic studies have been conducted on the dynamics of the forward and reverse reactions of NO with metalloporphyrins using various approaches such as time-resolved spectroscopic techniques, NO trapping methods, or NMR techniques.[4] In ferro- and ferri-heme proteins the occupation of the axial sites (e.g., by an imidazole nitrogen or a methionine sulfur) on the iron center can be responsible for a low reactivity toward NO, and protein conformational changes may account for additional complexities affecting protein reactivity in vivo. Thus, the formation of the nitrosyl complex of heme proteins may not only involve ligand displacement but also conformational changes. Also, the nitrosylation reaction of model metalloporphyrins in solution is affected by a number of different variables. Detailed studies on the activation parameters for the NO reaction in aqueous solution with iron(III) complexes of water soluble porphyrins have shown that the forward reaction is dominated by a dissociative step involving the breaking of an $Fe^{III}-OH_2$ bond,[5] similar factors accounting for the kinetics of $H_2O$ solvent exchange.[6] In compliance with microscopic reversibility, the dissociation of the nitrosyl complex is dominated by the solvent reorganization accompanying NO dissociation and concomitant spin change. The NO reaction with metMb showed similar activation parameters, demonstrating that water soluble ferri-heme complexes are suitable models for NO binding to metMb.[7] In contrast, the nitrosylation of model iron(II) porphyrin complexes does not seem to require the initial displacement of another ligand. This is verified not only in a weakly coordinating solvent such as toluene but also in water where rate constants are close to the diffusion limit.[5c] In general, these studies support the view that ferroporphyrin complexes and ferro-heme proteins react rapidly with NO because of a vacant or exceedingly labile coordination site.

In an effort to disentangle the complex role of the heme environment, the present work is aimed at gaining an insight into the neat interaction of NO with a heme center in an isolated state as provided by a low pressure gas phase. A thorough study on the addition of ligands to naked heme type ions is useful to gain an understanding of the factors governing the association process in solution or within the pocket of a heme protein. At the same time it may provide a closer view of the intrinsic properties of the ion.

The naked heme ion holding iron(III) coordinated by the dianion of protoporphyrin IX, henceforth named $[Fe^{III}$-heme$]^+$, is obtained in the gas phase in a straightforward way by electrospray ionization (ESI) of a solution of hemin chloride ($[Fe^{III}$-heme$]^+Cl^-$). Extensive work has been reported on the association of ligands to the vacant axial sites in $[Fe^{III}$-heme$]^+$, either by allowing the ion to react with a neutral in the gas phase[8] or by transferring preformed adducts from solution to the gas phase.[9] By the latter approach, the binding of $[Fe^{III}$-heme$]^+$ with nitrogen bases, antimalarial agents, and series of peptides has been described, probing ESI formed ions by energy-variable collision induced dissociation experiments.[9] On the basis of association equilibria studied in the gas phase by Fourier transform ion cyclotron resonance (FT-ICR) mass spectrometry, recent reports have shed light on the binding of $[Fe^{III}$-heme$]^+$ with nitric oxide and with a variety of exemplary ligands acting as models for the various functionalities that are present in a protein backbone.[8b] Obtaining a heme type cation holding iron(II) is less straightforward to achieve in the gas phase.[8a] In the present work an indirect approach is used, relying on the collision induced dissociation of the charged species from ESI of microperoxidase (MP11, the heme undecapeptide derived from enzymatic cleavage of cytochrome c).[10] The ion at *m*/*z* 617, displaying the characteristic isotopic pattern expected for the presence of an iron atom bound to the porphyrin ligand, corresponds formally to neutral $Fe^{II}$-heme with an excess unit positive charge resulting from the addition of a proton. The so-obtained species, henceforth named $[Fe^{II}$-hemeH$]^+$, has been investigated both computationally using density functional theory (DFT) and experimentally using FT-ICR mass spectrometry to study the ion chemistry toward hydrogen−deuterium exchange and a few exemplary ligand addition reactions.[10] In this way gaseous $[Fe^{II}$-hemeH$]^+$ ions have been characterized as species possessing iron(III) character to a certain extent because of partial electron transfer from the metal to the formally protonated vinyl group. The ion chemistry of $[Fe^{II}$-hemeH$]^+$ ions, however, shows notable differences with respect to the one displayed by $[Fe^{III}$-heme$]^+$. The comparative examination of the kinetics and thermodynamic parameters for the association reaction of the two ions to NO is reported in the present work. To this end, addition reactions involving a range of compounds have been inspected as well, allowing

(3) (a) Abu-Soud, H. M.; Ichimori, K.; Nakazawa, H.; Stuehr, D. J. *Biochemistry* **2000**, *40*, 6876. (b) Hurshman, A. R.; Marletta, M. A. *Biochemistry* **1995**, *34*, 5627. (c) Wang, J.; Rousseau, D. L.; Abu-Soud, H. M.; Stuehr, D. J. *Proc. Natl. Acad. Sci. USA* **1994**, *91*, 10512.

(4) (a) Wanat, A.; Wolak, M.; Orzel, L.; Brindell, M.; van Eldik, R.; Stochel, G. *Coord. Chem. Rev.* **2002**, *229*, 37. (b) Ford, P. C.; Lorkovic, I. M. *Chem. Rev.* **2002**, *102*, 993. (c) Hoshino, M.; Laverman, L.; Ford, P. C. *Coord. Chem. Rev.* **1999**, *187*, 75. (d) Macyk, W.; Franke, A.; Stochel, G. *Coord. Chem. Rev.* **2005**, *249*, 2437. (e) Lim, M. D.; Lorkovic, I. M.; Ford, P. C. *J. Inorg. Biochem.* **2005**, *99*, 151.

(5) (a) Laverman, L. E.; Hoshino, M.; Ford, P. C. *J. Am. Chem. Soc.* **1997**, *119*, 12663. (b) Laverman, L. E.; Ford, P. C. *Chem. Commun.* **1999**, 1843. (c) Laverman, L. E.; Ford, P. C. *J. Am. Chem. Soc.* **2001**, *123*, 11614.

(6) Schneppensierper, T.; Zahl, A.; van Eldik, R. *Angew. Chem., Int. Ed.* **2001**, *40*, 1678.

(7) Laverman, L. E.; Wanat, A.; Oszajca, J.; Stochel, G.; Ford, P. C.; van Eldik, R. *J. Am. Chem. Soc.* **2001**, *123*, 285.

(8) (a) Chen, O.; Groh, S.; Liechty, A.; Ridge, D. P. *J. Am. Chem. Soc.* **1999**, *121*, 11910. (b) Angelelli, F.; Chiavarino, B.; Crestoni, M. E.; Fornarini, S. *J. Am. Soc. Mass Spectrom.* **2005**, *16*, 589. (c) Crestoni, M. E.; Fornarini, S. *J. Biol. Inorg. Chem.* **2007**, *12*, 22. (d) Irikura, K. K.; Beauchamp, J. L. *J. Am. Chem. Soc.* **1991**, *113*, 2767–2768.

(9) (a) Vinokur, N.; Ryzhov, V. *J. Mass Spectrom.* **2004**, *39*, 1268. (b) Pashynska, V. A.; Van den Heuvel, H.; Claeys, M.; Kosevich, M. V. *J. Am. Soc. Mass Spectrom.* **2004**, *15*, 1181. (c) Hayes, L. A.; Chappell, A. M.; Jellen, E. E.; Ryzhov, V. *Int. J. Mass Spectrom.* **2003**, *227*, 111. (d) Jellen, E. E.; Ryzhov, V. *Eur. J. Mass Spectrom.* **2005**, *11*, 65. (e) Jellen, E. E.; Chappell, A. M.; Ryzhov, V. *Rapid Commun. Mass Spectrom.* **2002**, *16*, 1799.

(10) Chiavarino, B.; Crestoni, M. E.; Fornarini, S.; Rovira, C. *Chem. Eur. J.* **2007**, *13*, 776.

a scale of relative and absolute binding free energies to be established. In concert with experiment, DFT calculations have been undertaken to provide an independent source for the NO binding energies. The kinetic and thermodynamic data characterizing these isolated systems in the gas phase will be unaffected by additional factors caused by the presence of solvent, counterions, protein matrix, $\pi$-$\pi$ aggregates, and axial ligands.

## Results and Discussion

**Ligand Association to Gaseous [Fe$^{II}$-hemeH]$^+$.** When [Fe$^{II}$-hemeH]$^+$ ions extracted from the ESI source and isolated in the FT-ICR cell are exposed to a stationary concentration of selected neutral ligands (L), an addition reaction may be observed, leading to [Fe$^{II}$-hemeH(L)]$^+$. For the addition reaction between [Fe$^{II}$-hemeH]$^+$ and ligands such as NO and $(C_2H_5O)_3P$ the second order rate constants of 0.33 $\times$ $10^{-10}$ cm$^3$ molecule$^{-1}$ s$^{-1}$ and 4.0 $\times$ $10^{-10}$ cm$^3$ molecule$^{-1}$ s$^{-1}$, respectively, have been reported, as determined at 300 K.[10] In the present, thorough study, a vast array of compounds were tested and many were found unreactive, including biologically active diatomics ($O_2$ and CO), nitrogen bases ($NH_3$, $CH_3NH_2$, $CH_3CN$), carboxylic acids and derivatives (acetic acid, $CH_3C(O)N(CH_3)_2$), alcohols and ethers ($CH_3OH$, tetrahydrofuran, 2-methoxypropene), ketones ($(CH_3)_2CO$), and sulfides ($(CH_3)_2S$, $(CH_3)_2S_2$)). In relatively few cases, adduct ions are formed and the relevant thermodynamic features of the process are now reported. As depicted in eq 1, ligands such as $(CH_3)_2NH$, pyridine or $(CH_3O)_3PO$ do form adduct ions, although the reaction does not go to completion.

$$[Fe^{II}\text{-hemeH}]^+ + L \underset{k_r}{\overset{k_f}{\rightleftharpoons}} [Fe^{II}\text{-hemeH(L)}]^+ \qquad (1)$$

where L = $(CH_3)_2NH$, Pyridine, $(CH_3O)_3PO$. Rather, the temporal progress of the reaction leads to an unvarying ratio of the ion abundances for free [Fe$^{II}$-hemeH]$^+$ and [Fe$^{II}$-hemeH(L)]$^+$ ions, as shown in Figure 1a for L equal to $(CH_3O)_3PO$. The constant ion abundance ratio, $I$(Fe$^{II}$-hemeH(L)$^+$)/$I$(Fe$^{II}$-hemeH$^+$), that is observed at long reaction time, shows a linear dependence on the stationary pressure of the ligand, P(L), conforming to the behavior expected for an association equilibrium whose $K_1$ value responds to eq 2.

$$K_1 = \frac{I(Fe^{II}\text{-hemeH(L)}^+)}{I(Fe^{II}\text{-hemeH}^+) \times P(L)} \qquad (2)$$

Ion molecule association equilibria are not commonly met in FT-ICR mass spectrometry because of the prevailing low pressure conditions, an environment which does not favor attaining such equilibria. In fact, the ionic adduct, formed in a single collision event, retains primarily the energy released in its formation process. This excess energy may be dissipated only by radiative emission, the prevailing mechanism to reach thermal equilibrium in this low pressure regime,[11] because an alternative mechanism based on collisional stabilization is hindered here by the low frequency of third body collisions.[11] However, association equilibria in low pressure radiative association studies are met and described in a number of favorable instances.[8a,b,12,13] Both [Fe$^{III}$-heme]$^+$ and [Fe$^{II}$-hemeH]$^+$ ions under study share a similar, relatively large macrocyclic ligand characterized by the presence of strongly IR active groups. These features may account for an efficient thermal equilibration by rapid energy exchange with the background IR radiation field.[14] A further control that the constant $I$(Fe$^{II}$-hemeH(L)$^+$)/$I$(Fe$^{II}$-hemeH$^+$) ion abundance ratio at long reaction times fulfils the attainment of an association equilibrium rather than reflecting a kinetics steady state is gained by inspecting the approach to the ligand addition equilibrium from either the forward or the reverse direction. To this end, whereas Figure 1a shows the ion abundance profiles that are observed when [Fe$^{II}$-hemeH]$^+$ is allowed to react with $(CH_3O)_3PO$ at 2.6 $\times$ $10^{-8}$ mbar, in Figure 1b it is shown that the same final ion

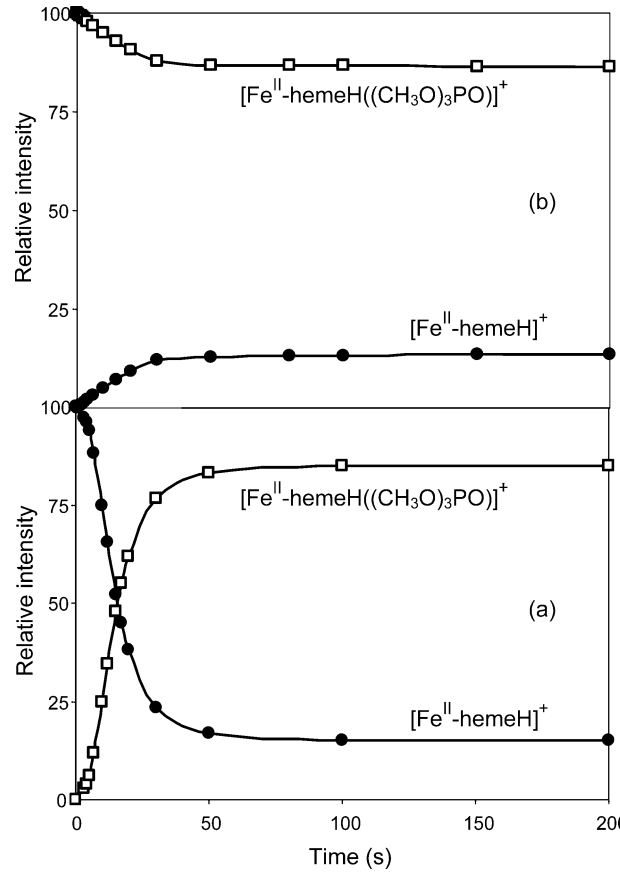


**Figure 1.** Time dependence of ion abundances when [Fe$^{II}$-hemeH]$^+$ ions are allowed to react with $(CH_3O)_3PO$ at 2.6 $\times$ $10^{-8}$ mbar (a). The upper portion (b) shows that at long reaction times the same ratio of ion abundances is observed when [Fe$^{II}$-hemeH((CH$_3$O)$_3$PO)]$^+$ adduct ions are isolated and then allowed to react (dissociate) under the same experimental conditions.

(11) (a) Dunbar, R. C. *Mass Spectrom. Rev.* **1992**, *11*, 309. (b) Fisher, J. J.; McMahon, T. B. *Int. J. Mass Spectrom. Ion Processes* **1990**, *100*, 701. (c) Dunbar, R. C. *Int. J. Mass Spectrom. Ion Processes* **1997**, *160*, 1.
(12) Fridgen, T. D.; McMahon, T. B. *J. Phys. Chem. A* **2002**, *106*, 1576.
(13) Ryzhov, V.; Dunbar, R. C. *J. Am. Soc. Mass Spectrom.* **1999**, *10*, 862.
(14) Price, W. D.; Williams, E. R. *J. Phys. Chem. A* **1997**, *101*, 8844.

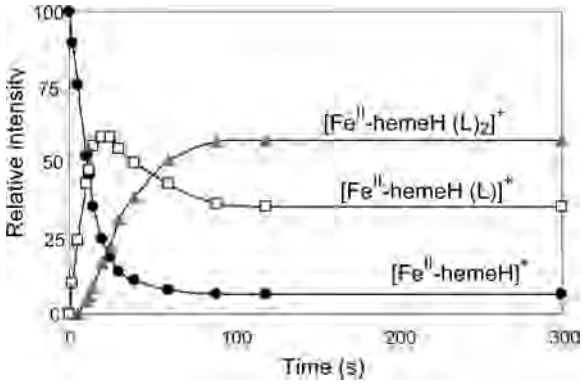


**Figure 2.** Time dependence of the relative ion abundances when selected [Fe$^{II}$-hemeH]$^+$ ions are allowed to react with L = $(CH_3)_2NH$ at $3.3 \times 10^{-7}$ mbar.

**Table 1.** Equilibrium Data for Ligand Addition Reactions to Gaseous [Fe$^{II}$-hemeH]$^+$ Ions

| L | $P^a$ | int. ratio$^b$ | $K_1$ ($\times 10^{-9}$)$^c$ |
|---|---|---|---|
| $(CH_3)_2NH$ | 33 | 5.1 | 15.7 |
| $(CH_3)_2NH$ | 7.8 | 1.13 | 14.7 |
| $(CH_3)_2NH$ | 18.5 | 2.3 | 12.6 |
| $(CH_3)_2NH$ | 6.4 | 1.10 | 17.4 |
| $(CH_3)_2NH$ | 11.5 | 1.8 | 15.6 |
| pyridine | 0.88 | 0.58 | 66.8 |
| pyridine | 2.0 | 1.23 | 62.3 |
| pyridine | 7.9 | 3.9 | 50.0 |
| pyridine | 10.2 | 7.7 | 76.5 |
| $(CH_3O)_3PO$ | 3.2 | 5.2 | 165 |
| $(CH_3O)_3PO$ | 1.9 | 3.4 | 181 |
| $(CH_3O)_3PO$ | 1.2 | 2.2 | 186 |

[a] Ligand pressure in units of $10^{-8}$ mbar. [b] $I$(Fe$^{II}$-hemeH(L)$^+$)/$I$(Fe$^{II}$-hemeH$^+$). [c] Standard state 1 atm; associative equilibrium constants for reaction (1) at 300 K.

abundance ratio is obtained when the adduct ion at *m*/*z* 757 is selected in the FT-ICR cell and allowed to undergo partial dissociation at the same pressure of $(CH_3O)_3PO$. The unvarying ratio of ion abundances that is observed when the kinetic progress of the reaction is over is evidence for an association equilibrium.

Whereas $(CH_3O)_3PO$ reacts by the addition of just one ligand molecule, the reaction of both $(CH_3)_2NH$ and pyridine proceeds toward a second addition step (eq 3) as illustrated by the temporal profiles of ion abundances shown in Figure 2. This consecutive reaction is slower than the first addition step so that eq 1 performs as a fast pre-equilibrium. The kinetic scheme is consistent with the decreasing abundances for [Fe$^{II}$-hemeH(L)]$^+$ and [Fe$^{II}$-hemeH]$^+$ ions because of the growing concentration of [Fe$^{II}$-hemeH(L)$_2$]$^+$, while their ratio has reached a value that remains constant at long reaction times.

Table 1 summarizes the $I$(Fe$^{II}$-hemeH(L)$^+$)/$I$(Fe$^{II}$-hemeH$^+$) ion abundance ratios when they attain constant values at varying ligand pressures together with the derived $K_1$ values. An increasing drive toward the formation of [Fe$^{II}$-hemeH(L)]$^+$ is observed in the series $(CH_3)_2NH$ < pyridine < $(CH_3O)_3PO$. The averaged $K_1$ values yield the corresponding $-\Delta G°_1$ values equal to 58.8, 62.4, and 65.0 (values expressed in kJ mol$^{-1}$, at 300 K; standard deviation is ± 0.5 kJ mol$^{-1}$) for $(CH_3)_2NH$, pyridine, and $(CH_3O)_3PO$, respectively. A still more pronounced thermodynamic drive toward association is displayed by other tested ligands, including the one of major interest in the present study, namely NO. Their reaction with [Fe$^{II}$-hemeH$^+$] leads to complete conversion of the free ion into [Fe$^{II}$-hemeH(L)]$^+$, thereby hampering a determination of $K_1$ by direct evaluation of the association equilibrium.

**Table 2.** Thermodynamic Data for the Ligand Transfer Reaction [Fe$^{II}$-hemeH(L$_1$)]$^+$ + L$_2$ ⇄ [Fe$^{II}$-hemeH(L$_2$)]$^+$ + L$_1$

| L$_1$ | L$_2$ | $K_3$[a] | $-\Delta G°_3$[b] |
|---|---|---|---|
| $(CH_3)_2NH$ | pyridine | 5.1 | 4.1 |
| pyridine | $(CH_3O)_3PO$ | 2.7 | 2.5 |
| $(CH_3O)_3PO$ | NO | 2.9 | 2.7 |
| pyridine | NO | 6.0 | 4.5 |
| $(CH_3)_2NH$ | NO | 27 | 8.3 |
| NO | $(CH_3O)_3P$ | 125 | 12.1 |

[a] Standard state 1 atm, 300 K. [b] kJ mol$^{-1}$. Standard deviation is ± 0.5 kJ mol$^{-1}$.

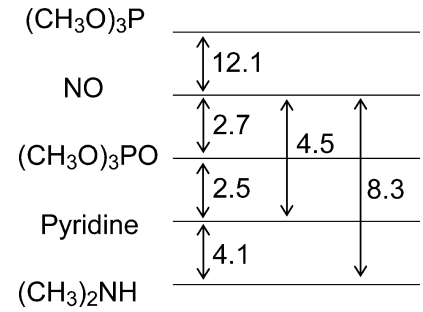


**Figure 3.** $\Delta G°_3$ (kJ mol$^{-1}$, 300K) ladder for the [Fe$^{II}$-hemeH]$^+$ transfer reactions between selected pairs of ligands. The values in the ladder correspond to H$^{II}$CB differences for each couple of ligands.

**Ligand Exchange Reactions.** When [Fe$^{II}$-hemeH$^+$] is allowed to react with a mixture of two reactive ligands, L$_1$ and L$_2$, both adduct ions are formed, [Fe$^{II}$-hemeH(L$_1$)]$^+$ and [Fe$^{II}$-hemeH(L$_2$)]$^+$, in relative amounts depending on the partial pressures of L$_1$ and L$_2$. A ligand transfer equilibrium is established (eq 3).

$$[\text{Fe}^{II}\text{-hemeH}(L_1)]^+ + L_2 \rightleftarrows [\text{Fe}^{II}\text{-hemeH}(L_2)]^+ + L_1 \quad (3)$$

$$K_3 = \frac{I(\text{Fe}^{II}\text{-hemeH}(L_2)^+) \times P(L_1)}{I(\text{Fe}^{II}\text{-hemeH}(L_1)^+) \times P(L_2)} \quad (4)$$

Ligand transfer equilibria, characterized by relatively modest enthalpy changes, are routinely studied by FT-ICR mass spectrometry.[15] The ratios of ion abundances, $I$(Fe$^{II}$-hemeH(L$_2$))$^+$ and $I$(Fe$^{II}$-hemeH(L$_1$))$^+$, obtained when [Fe$^{II}$-hemeH$^+$] is allowed to reach equilibrium in the presence of stationary concentrations of L$_1$ and L$_2$ in varying relative amounts, yield the equilibrium constant $K_3$ (eq 4) and the $\Delta G°_3$ values ($\Delta G°_3 = -RT \log K_3$) summarized in Table 2. The so obtained $\Delta G°_3$ values lend themselves to build a ladder of increasing thermodynamic drive to bind to [Fe$^{II}$-hemeH]$^+$, so that ultimately the least bound and the most effective ligand can be quantitatively compared. This ladder is depicted in Figure 3, spreading from $(CH_3)_2NH$ to $(CH_3O)_3P$, the most strongly bound among the sampled compounds. As shown in Figure 3, an overall good agreement is found by evaluating independent measurements. For example a $\Delta G°_3$ value of 4.5 kJ mol$^{-1}$ for L$_1$/L$_2$ equal to

(15) (a) McMahon, T. B. *Int. J. Mass Spectrom.* **2000**, *200*, 187. (b) Bartmess, J. E. *Mass Spectrom. Rev.* **1989**, *8*, 297.

**Table 3.** Free Energy Changes for Gas Phase Ligand Binding Towards $[Fe^{II}\text{-hemeH}]^+$ and $[Fe^{III}\text{-heme}]^+$

| Ligand | $H^{II}CB^a$ | $H^{III}CB^a$ | GB[b] |
|---|---|---|---|
| $CH_3NH_2$ | | 88.6[8b] | 865 |
| $(CH_3)_2NH$ | 58.8 | 97.9 | 897 |
| pyridine | 62.4 | 100.7[8b] | 898 |
| $(CH_3O)_3PO$ | 65.0 | 109.1[8b] | 861 |
| NO | 67.5 | 67.3[8b] | 505 |
| $(CH_3O)_3P$ | 79.6 | 102.4[8c] | 900 |

[a] $-\Delta G^\circ_1$ (named $H^{II}CB$) in kJ mol$^{-1}$ at 300 K. Values are also given for $H^{III}CB$, referred to the ligand association reaction toward $[Fe^{III}\text{-heme}]^+$. Estimated error ±0.5 kJ mol$^{-1}$ for relative values and ±4 kJ mol$^{-1}$ for absolute values. [b] Gas phase basicity (GB) in kJ mol$^{-1}$ at 298 K; data from ref 16.

NO/pyridine is reasonably matched by the 5.2 kJ mol$^{-1}$ sum of $\Delta G^\circ_3$ values for the equilibria involving NO/$(CH_3O)_3PO$ and $(CH_3O)_3PO$/pyridine (2.7 and 2.5 kJ mol$^{-1}$, respectively). The interest is focused on NO, and this ligand appears in the major number of ligand exchange equilibria reported in Table 2. However, the thermodynamic data collected for reactions 3 alone do not provide by themselves an absolute measure of the free energy change for NO binding to $[Fe^{II}\text{-hemeH}]^+$. To this end, one may rely on the simple association equilibria described by eq 1. Naming $Fe^{II}$−Heme Cation Basicity ($H^{II}CB$) the value of $-\Delta G^\circ_1$ for a selected ligand, one finds that $-\Delta G^\circ_3$ for a ligand exchange equilibrium equals the difference between $H^{II}CB(L_2)$ and $H^{II}CB(L_1)$. In this way averaged values for $H^{II}CB(L)$ can be obtained from the ligand transfer equilibria, when they are anchored to the $H^{II}CB$ values obtained for the association equilibria with $(CH_3)_2NH$, pyridine, and $(CH_3O)_3PO$. Once again, data from independent measurements are in fair agreement. For example, the reaction involving $(CH_3)_2NH$ ($L_1$) and pyridine ($L_2$) is characterized by $-\Delta G^\circ_3$ equal to 4.1 kJ mol$^{-1}$. This value is consistent with the difference in the respective $H^{II}CB(L)$ values which is equal to 3.6 kJ mole$^{-1}$. This finding provides support to the relationship expected to hold between $-\Delta G^\circ_3$ and the $H^{II}CB(L)$ values associated with the addition of $L_1$ and $L_2$, namely $-\Delta G^\circ_3 = H^{II}CB(L_2) - H^{II}CB(L_1)$. A similarly good matching is found when the $-\Delta G^\circ_3$ value of 2.5 kJ mol$^{-1}$for pyridine ($L_1$) and $(CH_3O)_3PO$ ($L_2$) is compared with the difference in their $H^{II}CB(L)$ which amounts to 2.6 kJ mol$^{-1}$. The internal consistency of the free energy change data in the ligand association (eq 1) and ligand exchange (eq 3) reactions confirms that $[Fe^{II}\text{-hemeH}]^+$ ions do partake in ligand association and ligand transfer equilibria under the prevailing experimental conditions. Table 3 gives a list of $H^{II}CB$ data. It also provides a comparison with $H^{III}CB$ data, as reported previously for the ligand association to $[Fe^{III}\text{-heme}]^+$ ions.[8b]

**Site of Ligand Attachment to $[Fe^{II}\text{-hemeH}]^+$.** It is conceivable that $[Fe^{II}\text{-hemeH}]^+$ ions may present other sites susceptible to attack by a base, besides the metal center. The protonated vinyl group at the periphery of the porphyrin macrocycle is such a candidate. It may conceivably engage in hydrogen bonding (a lone pair of the base interacting with a hydrogen atom on $C_\beta$) or in forming a Lewis adduct to an electrophilic carbon ($C_\alpha$ with respect to the porphyrin macrocycle). However, for a few reasons the direct attack to the protonated vinyl group appears unlikely, at least in the first addition event. The first striking piece of data emerging from Table 3 is the noticeable $H^{II}CB$ value displayed by NO. This molecule is a very weak base, as shown by the low value of its gas phase basicity (GB) toward the proton (GB values are listed in the last column of Table 3). Still, the $H^{II}CB$ value is remarkable, as expected for NO binding to the heme iron. A second consideration regards the trivalent phosphorus of $(CH_3O)_3P$ which is notably a poor partner in hydrogen bonding although this ligand is endowed with the highest $H^{II}CB$ among the tested compounds.[17] The relative trend of $H^{II}CB$ and $H^{III}CB$ showing an inversion for the couple $(CH_3O)_3P$/$(CH_3O)_3PO$, 79.6/65.0 kJ mol$^{-1}$ versus 102.4/109.1 kJ mol$^{-1}$, respectively, conforms rather to the expectation that the soft trivalent phosphorus ligand should display higher affinity for an iron(II) center.

As mentioned in a previous section, some ligands ($(CH_3)_2NH$, pyridine, and $(CH_3O)_3P$) display a tendency toward a second addition step leading to $[Fe^{II}\text{-hemeH}(L)_2]^+$. Whereas the combined evidence speaks in favor of a metal−ligand interaction for the first addition step, assigning the site for the second addition step appears less straightforward. There is precedent, though, for the formation of six-coordinate heme complexes in the gas phase.[8c] In particular, the $(CH_3O)_3P$ ligand displays unique properties in binding to $[Fe^{III}\text{-heme(L)}]^+$ (L equal to $(CH_3O)_3P$ or pyridine) at the sixth vacant coordination site. This feature was found promising to develop into a probe for testing the coordination environment of iron(III) within heme-peptide and heme-protein ions.[8c]

**Kinetic and Thermodynamic Parameters for the Binding of NO to $[Fe^{II}\text{-hemeH}]^+$ and $[Fe^{III}\text{-heme}]^+$ Ions.** Among the compounds listed in Table 3 together with their respective thermodynamic data for the association to heme ions, NO shows a quite distinct behavior. It displays remarkable binding properties toward both $[Fe^{II}\text{-hemeH}]^+$ and $[Fe^{III}\text{-heme}]^+$ ions. This point is evident, for example, in the approximate relationship that was found to hold between $H^{III}CB$ and GB values for an extensive and varied list of ligands,[8b] where the $H^{III}CB$ value for NO is by far greater than the one predicted along the approximate correlation line. The failure of GB values to provide an indicator for relative binding free energy to heme type ions is even more evident in the case of $[Fe^{II}\text{-hemeH}]^+$ ions. For example, the performance of $(CH_3O)_3P$ as a ligand largely exceeds the one displayed by $(CH_3)_2NH$ and pyridine in spite of their approximately equal gas phase basicity. Beyond being an exceptional ligand, it is also striking that NO shows very similar values for the binding free energies to both $[Fe^{II}\text{-hemeH}]^+$ and $[Fe^{III}\text{-heme}]^+$ ions, practically the same HCB within the experimental error. Because also the bimolecular rate constants for the association reaction ($k_f$ in eq 1) share very close values, $3.3 \times 10^{-11}$ cm$^3$ molecule$^{-1}$ s$^{-1}$ and 2.2

(16) Hunter, E. P.; Lias, S. G. In *NIST Chemistry Webbook, NIST Standard Reference Database Number 69*; Linstrom, P. J., Mallard, W. G., Eds.; National Institute of Standards and Technology: Gaithersburg, MD, 2005; http://webbook.nist.gov.
(17) Meot-Ner, M. *Chem. Rev.* **2005**, *105*, 213.

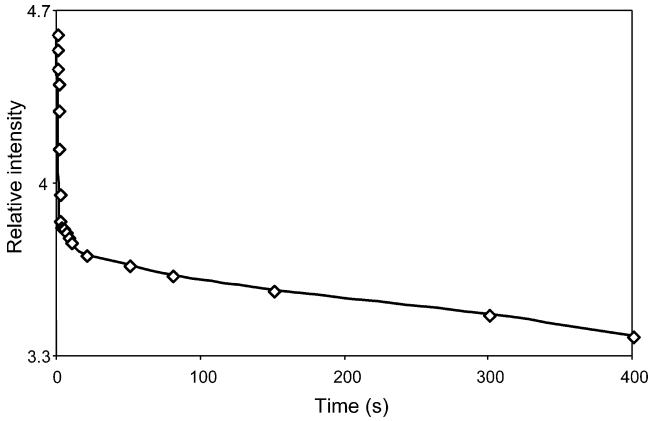


**Figure 4.** Semilogarithmic plot of the relative ion abundance of the NO adduct of $[Fe^{II}\text{-hemeH}]^+$ ions undergoing ligand dissociation when led into the degassed FT-ICR cell ($P < 4 \times 10^{-9}$ mbar) and isolated by rf shots.

$\times 10^{-11}$ cm$^3$ molecule$^{-1}$ s$^{-1}$ for $[Fe^{II}\text{-hemeH}]^+$ and $[Fe^{III}\text{-heme}]^+$ ions,[8b,10] respectively, closely similar rate constants are expected also for the dissociation of the nitrosyl adducts ($k_r$ in eq 1). Incidentally, one may note a fair agreement between the $k_f$ value of $2.2 \times 10^{-11}$ cm$^3$ molecule$^{-1}$ s$^{-1}$ for $[Fe^{III}\text{-heme}]^+$ binding to NO and the $1.5 \times 10^{-11}$ cm$^3$ molecule$^{-1}$ s$^{-1}$ value reported in the landmark paper by Ridge et al.[8a] For $[Fe^{II}\text{-hemeH}]^+$, taking into account the $H^{II}CB$ of NO, one obtains a $K_1$ value of $5.7 \times 10^{11}$ (standard state 1 atm) at 300 K. Equating $K_1$ to the rate constant ratio $k_f/k_r$, a $k_r$ rate constant of $1.4 \times 10^{-3}$ s$^{-1}$ is evaluated. This estimated rate constant for the unimolecular dissociation of $[Fe^{II}\text{-hemeH(NO)}]^+$ complexes can be tested directly by experiment. To this end, $[Fe^{II}\text{-hemeH(NO)}]^+$ ions were formed by exposing $[Fe^{II}\text{-hemeH}]^+$ formed in the ESI source to NO gas. The nitrosyl adducts were led into the FT-ICR cell where they were isolated using low energy rf shots. The time dependence of the $[Fe^{II}\text{-hemeH(NO)}]^+$ ion abundance is displayed in the semilog plot of Figure 4 which shows a fast dissociation process followed by a slow one. The bimodal decay is ascribed to the presence of a fraction of excited $[Fe^{II}\text{-hemeH(NO)}]^+$ ions, due to the transfer and/or the isolation process (or, possibly, due to the presence of an isolated electronic state), together with thermally equilibrated species which are responsible for the slow dissociation reaction. When the $[Fe^{II}\text{-hemeH(NO)}]^+$ ion population is submitted to collisional cooling by application of an argon pulse followed by a delay time to remove the gas from the cell, the fast reacting fraction disappears, as expected. The time constant for the slow dissociation reaction is $0.8 \times 10^{-3}$ s$^{-1}$. This value differs only by a factor of about two from the $k_r$ rate constant of $1.4 \times 10^{-3}$ s$^{-1}$ evaluated from the ratio $k_f/K_1$. These data appear then in fair agreement. The set of $K_1$, $k_f$, and $k_r$ values, each obtained by an independent measurement, are summarized in Table 4. In a similar experiment, a $k_r$ value of $0.9 \times 10^{-3}$ s$^{-1}$ can be obtained for the unimolecular decay of $[Fe^{III}\text{-heme(NO)}]^+$ ions. Once again this value can be compared with an expected $k_r$ of $1.0 \times 10^{-3}$ s$^{-1}$, as evaluated from the $k_f/K_1$ ratio for the association reaction of NO to $[Fe^{III}\text{-heme}]^+$ ions. For this species the agreement is still closer. The parameters for the association of NO to both $[Fe^{II}\text{-hemeH}]^+$ and $[Fe^{III}\text{-heme}]^+$ collected in Table 4 provide a comprehensive picture of the kinetics and equilibrium data regarding the elementary association of NO to genuine, four-coordinate $Fe^{II}$- or $Fe^{III}$-heme ions. It may be noted that a four-coordinate iron(III) porphyrin cation has been obtained in condensed phase only recently by using an extremely hindered bis-pocket siloxyl porphyrin.[18]

**Table 4.** Kinetics and Equilibrium Data for NO Binding to $[Fe^{II}\text{-hemeH}]^+$ and $[Fe^{III}\text{-heme}]^+$ Ions in the Gas Phase

| reagent ion | $K_1$ ($\times 10^{-11}$)[a] | $k_f$ ($\times 10^{11}$)[b] | $k_r$ ($\times 10^{3}$)[c] |
|---|---|---|---|
| $[Fe^{II}\text{-hemeH}]^+$ | 5.7 | 3.3 | 0.8 |
| $[Fe^{III}\text{-heme}]^+$ | 5.3 | 2.2 | 0.9 |

[a] Equilibrium constant for the association of NO to the heme ions at 300 K, obtained from the $H^{II}CB/H^{III}CB$ values reported in Table 3 ($K_1$ = exp(HCB/RT)). Standard state 1 atm. [b] Forward rate constant for the association of NO to the heme ions, in units of cm$^3$ molecule$^{-1}$ s$^{-1}$, at 300 K. refs 8b and 10. [c] Reverse rate constant for the association of NO to the heme ions, in s$^{-1}$, at 300 K. This work.

**Binding Energies of the $[Fe^{III}\text{-heme(NO)}]^+$ and $[Fe^{II}\text{-hemeH(NO)}]^+$ Complexes.** To obtain further insight into the binding properties of NO to naked iron(II)- or iron(III)-heme ions, the energy released in the association process has been calculated by Density Functional Theory (DFT). This method is the preferred computational approach for sizable organometallic systems.[19,20] In a recent study, a comprehensive evaluation of various computational methods has confirmed an intermediate spin state to be the ground-state for both the iron(II) and the iron(III) porphyrins, namely a triplet and a quartet, respectively.[20b] Quantum chemical calculations were typically based on iron (II/III) porphine complexes ($[Fe^{II/III}\text{-P}]^{0/+1}$ computational models, where P is the dianion of porphine) because of computational limitations brought about by the fully substituted heme systems.[21] This choice was justified by noting that the electronic properties of the complex are expected to be insensitive to the presence and nature of peripheral substituents.[21c,22] A similar simplified model was adopted in characterizing the structural, electronic, and spectroscopic features of iron porphyrin-NO

(18) Fang, M.; Wilson, S. R.; Suslick, K. S. *J. Am. Chem. Soc.* **2008**, *130*, 1134.
(19) (a) Siegbahn, P. E. M.; Borowski, T. *Acc. Chem. Res.* **2006**, *39*, 729. (b) Baerends, E. J.; Ricciardi, G.; Rosa, A.; van Gisbergen, S. J. A. *Coord. Chem. Rev.* **2002**, *230*, 5.
(20) (a) Ghosh, A. *J. Biol. Inorg. Chem.* **2006**, *11*, 712. (b) Groenhof, A. R.; Swart, M.; Ehlers, A. W.; Lammertsma, K. *J. Phys. Chem. A* **2005**, *109*, 3411.
(21) (a) Shaik, S.; Hirao, H.; Kumar, D. *Acc. Chem. Res.* **2007**, *40*, 532. (b) Romanova, T. A.; Krasnov, P. O. *Chem. Phys. Lett.* **2006**, *420*, 281. (c) Liao, M. -S.; Scheiner, S. *J. Comput. Chem.* **2002**, *23*, 1391. (d) Ugalde, J. M.; Dunietz, B.; Dreuw, A.; Head-Gordon, M.; Boyd, R. J. *J. Phys. Chem. A* **2004**, *108*, 4653–4657. (e) Rydberg, P.; Sigfridsson, E.; Ryde, U. *J. Biol. Inorg. Chem* **2004**, *9*, 203. (f) Scherlis, D. A.; Cymeryng, C. B.; Estrin, D. A. *Inorg. Chem.* **2000**, *39*, 2352. (g) Rovira, C.; Carloni, P.; Parrinello, M. *J. Phys. Chem. B* **1999**, *103*, 7031. (h) Rovira, C.; Ballone, P.; Parrinello, M. *Chem. Phys. Lett.* **1997**, *271*, 247. (i) Smith, D. M. A.; Dupuis, M.; Vorpagel, E. R.; Straatsma, T. *J. Am. Chem. Soc.* **2003**, *125*, 2711. (j) Kozlowski, P. M.; Spiro, T. G.; Berces, A.; Zgierski, M. Z. *J. Phys. Chem. B* **1998**, *102*, 2603. (k) Marechal, J. -D.; Barea, G.; Maseras, F.; Lledos, A.; Mouawad, L.; Perahia, D. *J. Comput. Chem.* **2000**, *21*, 282. (l) Matsuzawa, N.; Ata, M.; Dixon, D. A. *J. Phys. Chem.* **1995**, *99*, 7698. (m) Delley, B. *Physica B* **1991**, *172*, 185.
(22) (a) Johansson, M. P.; Sundholm, D.; Gerfen, G.; Wikstroem, M. *J. Am. Chem. Soc.* **2002**, *124*, 11771. (b) Rovira, C.; Parrinello, M. *Chem. Eur. J.* **1999**, *5*, 250.

complexes.[23] More recently, DFT calculations have addressed the geometric and electronic structure of the isolated heme molecule, [$Fe^{II}$-heme] and its positive ion, [$Fe^{III}$-heme]$^+$,[22b,24] besides the protonated species, [$Fe^{II}$-hemeH]$^+$.[10] In the present context, the binding energy of NO to both [$Fe^{II}$-hemeH]$^+$ and [$Fe^{III}$-heme]$^+$, the species studied for NO addition in the gas phase experiments, has been evaluated using DFT. To this end the electronic energies for all species partaking in eqs 5 and 6 have been calculated for the optimized structures in the electronic ground state. The optimized structure of [$Fe^{II}$-hemeH]$^+$ in the triplet ground-state has already been reported.[10] The geometry of [$Fe^{III}$-heme]$^+$ has been optimized in the quartet ground state[24a,b] and a list of structural parameters is provided in the Supporting Information, Table S1. The reaction with NO (doublet) gives strong field, low spin nitrosyl complexes[4b,24] and a doublet and a singlet ground-state are expected for the NO complexes with [$Fe^{II}$-hemeH]$^+$ and [$Fe^{III}$-heme]$^+$, respectively.[20a,23b,k−p] In the NO complexes any formal assignment to the metal oxidation state is problematic because considerable charge transfer between the NO ligand and the metal can occur.[4b,25,26]

$$[Fe^{II}\text{-hemeH}]^+ + NO \underset{k_r}{\overset{k_f}{\rightleftharpoons}} [Fe^{II}\text{-hemeH(NO)}]^+ \qquad (5)$$

$$[Fe^{III}\text{-heme}]^+ + NO \underset{k_r}{\overset{k_f}{\rightleftharpoons}} [Fe^{III}\text{-heme(NO)}]^+ \qquad (6)$$

Limiting geometries are expected where the Fe−N−O angles are approximately linear (170−180°) or bent (140−150°), as observed for a variety of five coordinate "ferrous" nitrosyl complexes and "ferric" derivatives in the solid state.[25,27] The optimized geometries of [$Fe^{II}$-hemeH(NO)]$^+$ and [$Fe^{III}$-heme(NO)]$^+$ shown in Figures 5 and 6 conform to these expectations. In both cases the NO is attached in the $\eta^1$-NO configuration and the porphyrin core has approximately $C_s$ symmetry. Alternative $\eta^1$-ON (isonitrosyl), and $\eta^2$-NO (side-on bound NO) linkage isomers are known to lie quite higher in energy, when located in a potential energy minimum.[23a−d,27b,e] Notable features of the equilibrium geometry of [$Fe^{II}$-hemeH(NO)]$^+$ are the Fe−N and N−O bond distances of 1.71 and 1.18 Å, respectively, and the Fe−N−O angle of 145.6°. NO is oriented toward the meso C-atom of the porphyrin ring, with a small tilting of the Fe−$N_{NO}$ axis with respect to the orthogonal to the porphyrin frame passing through Fe atom (4.6°). The NO ligand pulls the iron atom upward by 0.25 Å with respect to the plane defined by the porphyrin nitrogen atoms. As shown in Figure 7, the spin density distribution is localized mainly on iron in the $d_{z^2}$ orbital, characterizing the metal as a doublet spin state, while residual spin density on NO has zero integral.

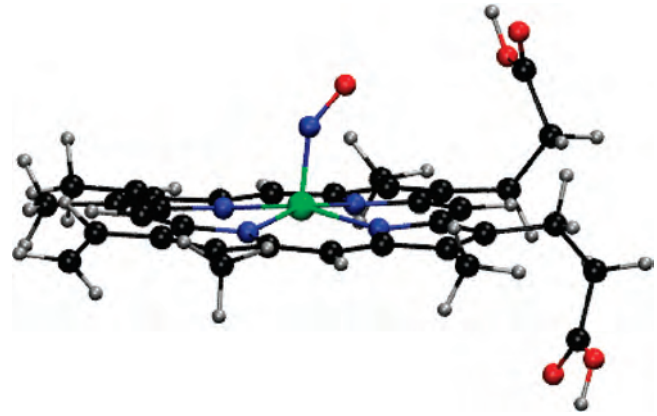

**Figure 5.** Optimized structure of [$Fe^{II}$-hemeH(NO)]$^+$.

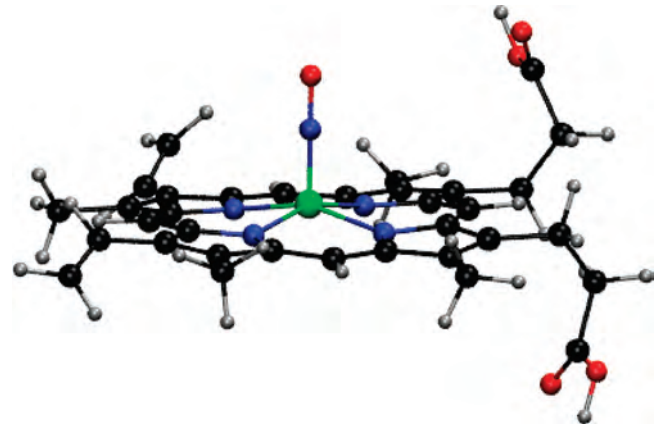

**Figure 6.** Optimized structure of [$Fe^{III}$-heme(NO)]$^+$.

(23) (a) Ghosh, A. *Acc. Chem. Res.* **2005**, *38*, 943. (b) Wondimagegn, T.; Ghosh, A. *J. Am. Chem. Soc.* **2001**, *123*, 5680. (c) Nutt, D. R.; Meuwly, M. *ChemPhysChem* **2007**, *8*, 527. (d) Nutt, D. R.; Karplus, M.; Meuwly, M. *J. Phys. Chem. B* **2005**, *109*, 21118. (e) Paulat, F.; Lehnert, N. *Inorg. Chem.* **2007**, *46*, 1547. (f) Blomberg, L. M.; Blomberg, M. R. A.; Siegbahn, P. E. M. *J. Inorg. Biochem.* **2005**, *99*, 949. (g) Ibrahim, M.; Xu, C.; Spiro, T. G. *J. Am. Chem. Soc.* **2006**, *128*, 16834. (h) Vogel, K. M.; Kozlowski, P. M.; Zgierski, M. Z.; Spiro, T. J. *J. Am. Chem. Soc.* **1999**, *121*, 9915. (i) Marti, M. A.; Capece, L.; Crespo, A.; Doctorovich, F.; Estrin, D. A. *J. Am. Chem. Soc.* **2005**, *127*, 7721. (j) Linder, D. P.; Rodgers, K. R. *Inorg. Chem.* **2005**, *44*, 1367. (k) Linder, D. P.; Rodgers, K. R.; Banister, J.; Wyllie, G. R. A.; Ellison, M. K.; Scheidt, W. R. *J. Am. Chem. Soc.* **2004**, *126*, 14136. (l) Zhang, Y.; Gossman, W.; Oldfield, E. *J. Am. Chem. Soc.* **2003**, *125*, 16387. (m) Franzen, S. *Proc. Natl. Acad. Sci. U.S.A.* **2002**, *99*, 16754. (n) Roberts, S. A.; Weichsel, A.; Qiu, Y.; Shelnutt, J. A.; Walker, F. A.; Montfort, W. R. *Biohemistry* **2001**, *40*, 11327. (o) Patchkovskii, S.; Ziegler, T. *Inorg. Chem.* **2000**, *39*, 5354. (p) Rovira, C.; Kunc, K.; Hutter, J.; Ballone, P.; Parrinello, M. *J. Phys. Chem. A* **1997**, *101*, 8914. (q) Rovira, C.; Kunc, K.; Hutter, J.; Ballone, P.; Parrinello, M. *Int. J. Quantum Chem.* **1998**, *69*, 31. (r) Bikiel, D. E.; Bari, S. E.; Doctorovich, F.; Estrin, D. A. *J. Inorg. Biochem.* **2008**, *102*, 70.

(24) (a) Charkin, O. P.; Klimenko, N. M.; Charkin, D. O.; Chang, H. -C.; Lin, S.-H. *J. Phys. Chem. A* **2007**, *111*, 9207. (b) Charkin, O. P.; Klimenko, N. M.; Nguyen, P. T.; Charkin, D. O.; Mebel, A. M.; Lin, S. H.; Wang, Y. - S.; Wei, S.-C.; Chang, H.-C. *Chem. Phys. Lett.* **2005**, *415*, 362. (c) Siu, C.-K.; Guo, Y. C.; Hopkinson, A.; Siu, K. W. M. *J. Phys. Chem. B* **2006**, *110*, 24207.

(25) (a) Wyllie, G. R. A.; Scheidt, W. R. *Chem. Rev.* **2002**, *102*, 1067. (b) Scheidt, W. R.; Ellison, M. K. *Acc. Chem. Res.* **1999**, *32*, 350.

(26) Enemark, J. H.; Feltham, R. D. *Coord. Chem. Rev.* **1974**, *13*, 339.

(27) (a) Richter-Addo, G. B.; Wheeler, R. A.; Hixson, C. A.; Chen, L.; Khan, M. A.; Ellison, M. K.; Schulz, C. E.; Scheidt, W. R. *J. Am. Chem. Soc.* **2001**, *123*, 6314. (b) Lee, J.; Kovalevsky, A. Y.; Novozhilova, I. V.; Bagley, K. A.; Coppens, P.; Richter-Addo, G. B. *J. Am. Chem. Soc.* **2004**, *126*, 7180. (c) Copeland, D. M.; Soares, A. S.; West, A. H.; Richter-Addo, G. B. *J. Biol. Inorg. Chem.* **2006**, *100*, 1413. (d) Xu, N.; Powell, D. R.; Cheng, L.; Richter-Addo, G. B. *Chem. Commun.* **2006**, 2030. (e) Novozhilova, I. V.; Coppens, P.; Lee, J.; Richter-Addo, G. B.; Bagley, K. A. *J. Am. Chem. Soc.* **2006**, *128*, 2093.

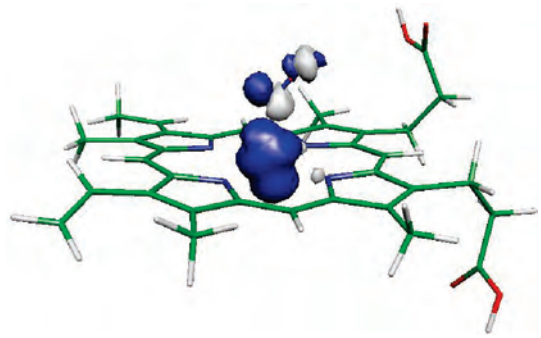

**Figure 7.** Spin density of $[Fe^{II}\text{-hemeH(NO)}]^+$.

This feature makes an interesting contrast with the spin density distribution in $[Fe^{II}\text{-hemeH}]^+$ where an appreciable fraction is located on the peripheral, formally protonated, vinyl group, conferring radical character to this group.[10] The so-obtained description of $[Fe^{II}\text{-hemeH(NO)}]^+$ is consistent with that of an iron(II)-heme bound to NO. A binding energy of 140 kJ mol$^{-1}$ is calculated with respect to dissociation into triplet $[Fe^{II}\text{-hemeH}]^+$ and $^2$NO. This value is remarkably close to the 146 and 142 kJ mol$^{-1}$ binding energies reported for the neutral $Fe^{II}-P(NO)$ and $Fe^{II}$-heme(NO) complexes, respectively.[22b,23p] The equilibrium geometry of $[Fe^{III}\text{-heme(NO)}]^+$ depicted in Figure 6 is characterized by Fe−N and N−O bond distances of 1.61 and 1.17 Å, respectively, and by the Fe−N−O angle of 178.6°, with an upward displacement of iron relative to the porphyrin nitrogens equal to 0.36 Å. The calculated binding energy is 144 kJ mol$^{-1}$ with respect to quartet $[Fe^{III}\text{-heme}]^+$ and $^2$NO. Overall, the computational results indicate that the energies involved in the binding of NO to iron(II)- and iron(III)-hemes in the gas phase are practically the same.

**Comparative Binding Of NO to Naked Iron(II)- and Iron(III)-Heme Ions.** Aiming to assess the binding properties of NO to naked iron(II)- and iron(III)-heme ions, a combined approach was adopted to obtain both experimental data on the thermodynamics of the association equilibria in the gas phase and computational data on the absolute binding energies regarding the same species probed in the mass spectrometric study. On the experimental side it is found that the free energy for NO binding to $[Fe^{II}\text{-hemeH}]^+$ and $[Fe^{III}\text{-heme}]^+$ is −67.5 and −67.3 kJ mol$^{-1}$ at 298 K (Table 3), respectively, which means that the two ions share a practically common $\Delta G°$ value. Subtracting the approximate entropy loss for NO binding estimated by statistical thermodynamics ($\Delta S = -190$ J K$^{-1}$ mol$^{-1}$)[8a] one obtains the NO binding energy of 124 kJ mol$^{-1}$ (namely $-\Delta H°$ for reactions 5 and 6). This datum may be compared with an independent experimental evaluation of the NO binding energy to $[Fe^{III}\text{-heme}^+]$ based on radiative association kinetics, which yielded a binding energy of 104 kJ mol$^{-1}$.[8a] On the computational side, the NO binding energies to $[Fe^{II}\text{-hemeH}]^+$ and $[Fe^{III}\text{-heme}]^+$ yield once again values that are virtually the same (140 and 144 kJ mol$^{-1}$, respectively), although the structural and electronic features of the nitrosyl adducts clearly pertain to distinct complexes. Also striking is the similarity of the kinetic parameters for NO binding and dissociation. The $k_f$ rate constant is $3.3 \times 10^{-11}$ and $2.2 \times 10^{-11}$ cm$^3$ molecule$^{-1}$ s$^{-1}$ for NO binding to $[Fe^{II}\text{-hemeH}]^+$ and $[Fe^{III}\text{-heme}]^+$, respectively (Table 4 and ref 10). These very close values are still well below the collisional rate constant of about $7.4 \times 10^{-10}$ cm$^3$ molecule$^{-1}$ s$^{-1}$,[28] meaning that the addition process is not collision limited and the rate constant is controlled by chemical reactivity. In fact, a ligand as powerful as $(C_2H_5O)_3PO$ is required for the addition reaction with $[Fe^{III}\text{-heme}]^+$ to proceed on every collision event.[10] The rates for NO dissociation, activated by the background IR radiation field,[14,29] are $0.8 \times 10^{-3}$ and $0.9 \times 10^{-3}$ s$^{-1}$ (Table 4), displaying once again values that are equal within experimental error.

The present findings on the gas phase characteristics of "ferrous" and formally "ferric" heme derivatives may be evaluated with respect to the binding of NO to heme proteins and their model complexes in solution. The rate constants, $k_f$, for the association of NO are typically very high, being significantly larger for the ferrous complexes. This behavior has been ascribed to the requisite of either a very labile or a vacant coordination site on the metal for a facile addition of NO to occur. This condition is verified in high spin iron(II)-heme proteins which show also the largest values for the association equilibrium constants.[4] For example, the respective $K$ values for the association of NO to iron(II)-myoglobin and iron(III)-metmyoglobin differ by a factor as large as $10^7$ resulting from a higher value of $k_f$ and a lower value for the dissociation rate constant, $k_r$, both favoring the stability of the "ferrous" nitrosyl complex. The binding of NO to the $Fe^{III}$-heme center of metmyoglobin has been described by eq 7

$$\text{metMb}(H_2O) + NO \underset{k_r}{\overset{k_f}{\rightleftharpoons}} \text{metMb(NO)} + H_2O \qquad (7)$$

Detailed kinetic and mechanistic studies on the binding of NO to metmyoglobin and to model Fe(III) complexes have revealed large and positive activation entropies and activation volumes pointing to a dissociative ligand substitution mechanism for both binding and release of NO. The reactions are further complicated by the solvent reorganization associated with bond breakage and charge redistribution accompanying the low spin−high spin transformation at the metal. In a recent, important contribution to the thermodynamic and kinetic studies of NO binding to heme proteins, a model iron(III) complex for the P450 enzyme has been examined both in toluene and in methanol solution.[30] The nitrosylation reaction in noncoordinating toluene was found to conform to a mechanism dominated by bond formation associated to spin change in the binding of NO. In contrast, the reaction in methanol was found to be much slower, requiring solvent displacement from a six-coordinate iron(III) complex.

The iron(II/III)-heme ions examined in the dilute gas phase present an ultimate effort toward highly simplified com-

(28) Su, T.; Chesnavich, W. J. *J. Chem. Phys.* **1982**, *76*, 5183.
(29) (a) Dunbar, R. C.; McMahon, T. B. *Science* **1998**, *279*, 194. (b) Price, W. D.; Schnier, P. D.; Williams, E. R. *Anal. Chem.* **1996**, *68*, 859.
(30) Franke, A.; Stochel, G.; Suzuki, N.; Higuchi, T.; Okuzono, K.; van Eldik, R. *J. Am. Chem. Soc.* **2005**, *127*, 5360.

plexes, both being four-coordinate iron-porphyrin complexes, lacking any perturbation by axial ligands or solvent molecules. Under these conditions iron(II/III)-hemes can display their intrinsic kinetic and thermodynamic properties, showing an unprecedented, remarkable similarity in the kinetic and thermodynamic parameters affecting their association reaction to NO.

## Conclusion

Assessing the intrinsic features for NO binding to iron(II/III)-hemes under conditions where the two species could share the same environment and be least affected by external factors was the aim of the present work. The low pressure gas phase within an FT-ICR cell provided a suitable medium, allowing binding free energies and rate constants for the forward and reverse reactions to be determined. The somewhat unexpected, striking result was to find that both naked $[Fe^{II}\text{-hemeH}]^+$ and $[Fe^{III}\text{-heme}]^+$ ions display virtually the same behavior in their kinetic and thermodynamic parameters for NO binding. For example, the equilibrium constant for the association of NO is $5.7 \times 10^{11}$ and $5.3 \times 10^{11}$ for $[Fe^{II}\text{-hemeH}]^+$ and $[Fe^{III}\text{-heme}]^+$, respectively. The properties manifested in the experimental study find a correspondence in the binding energies obtained by DFT calculations. The computed NO binding energies to $[Fe^{II}\text{-hemeH}]^+$ and $[Fe^{III}\text{-heme}]^+$ (140 and 144 kJ mol$^{-1}$, respectively) confirm that the two ions have a similarly pronounced affinity toward this diatomic messenger molecule. In contrast, the *K* values for the reaction of NO with representative heme proteins and model iron(II/III) porphyrin complexes in solution may differ by several orders of magnitude.[4] This finding definitely points out that the distinct behavior of the "ferrous" and "ferric" nitrosyl complexes in solution or in biological environments arises from coordination and/or solvation effects, underlying the important role played by a vacant or labile coordination site. As a final comment one may concur in stating with Ford and his co-workers that "the mechanism (and rates) for NO substitution into the iron centers is more defined by the coordination number than the oxidation state".[31] For the naked $[Fe^{II}\text{-hemeH}^+]$ and $[Fe^{III}\text{-heme}^+]$ ions this statement does indeed hold and is consistent with the observed features of the gas phase reaction. As a general comment one may note that the gas phase ion chemistry of transition metal complexes may provide valuable insights for mechanistic studies in solution.[32]

## Experimental Section

**Mass Spectrometric Experiments.** All experiments were performed by using an FT-ICR Bruker Spectrospin 47e mass spectrometer upgraded to BioApex with an Analytica of Branford ESI source. ESI-formed ions are led into a cylindrical "infinity" cell within a 4.7 T magnet. The nominal base pressure is typically around $2 \times 10^{-9}$ mbar, and neutral compounds may be leaked through needle valves, up to constant pressures in the range of $1.0-12 \times 10^{-8}$ mbar. The pressure is measured with a cold cathode sensor (IKR Pfeiffer Balzers S.p.A., Milan, Italy). The pressure readings were corrected for the sensitivity of the sensor toward each neutral compound[33] and for the pressure gradient between the cell and the sensor. The latter correction was achieved by measuring the rates of exothermic proton and electron transfer reactions involving the neutral molecules of interest.[34] In particular, the charge transfer reaction of $CO_2^+$ with NO was used to calibrate the NO pressure. Ion ejection routines as commonly performed in FT-ICR mass spectrometry were used to select the reagent ion and observe the ion chemistry with the neutral admitted into the cell. To avoid unintended off-resonance excitation of the reactant ion, the whole isotopic cluster corresponding to the iron(II/III)-heme ion was isolated and allowed to react with the selected neutral. Single radiofrequency pulses were used to eject other ions. The reactions were studied under conditions responding to either first order or pseudo first order kinetics, and rate constants were obtained from the semilogarithmic plot of the relative abundance of the reactant ion versus time. Ligand addition and ligand exchange equilibria were examined allowing a long enough reaction time to ensure the attainment of constant relative ion abundances for the species involved.

The ions of interest were produced in the gas phase by ESI of 10 $\mu$M solutions containing either hemin chloride in methanol or microperoxidase (MP11) in 1:1 aqueous methanol containing 2% acetic acid. The solutions were sprayed at a 2 $\mu$L min$^{-1}$ flow rate controlled by a syringe pump. A countercurrent flow of heated dry gas (nitrogen at 130 °C) was used to desolvate the ions. After an accumulation interval of 0.5 s in a rf-only hexapole, the ion population was pulsed into the ICR cell at room temperature (300 K). ESI of hemin chloride yields gaseous $[Fe^{III}\text{-heme}]^+$ ions at nominal *m/z* 616, whereas $[Fe^{II}\text{-hemeH}]^+$ ions (*m/z* 617) are obtained by collision induced dissociation of MP11 ions applying a high capillary to skimmer potential difference.

All compounds were from commercial sources (Sigma-Aldrich Co.; Matheson Gas Co.) and used as received.

**Computational Details.** The initial structures for the calculation of $[Fe^{II}\text{-hemeH(NO)}]^+$ and $[Fe^{III}\text{-heme(NO)}]^+$ were taken from the optimized structure of $[Fe^{II}\text{-hemeH}]^+$ and $Fe^{II}$-heme, respectively, obtained in our previous works.[10,22b] The NO ligand was bound initially in an end-on configuration, as in $Fe^{II}$-heme. [22b] The $[Fe^{II}\text{-hemeH(NO)}]^+$ and $[Fe^{III}\text{-heme(NO)}]^+$ complexes were optimized in their lowest energy spin state, which turned out to be the doublet and singlet, respectively. Binding energies were computed by comparing the total energy of the complex with those of the optimized fragments in their lowest energy spin state. The corresponding species were considered: $[Fe^{II}\text{-hemeH}]^+$ (triplet),[10] $[Fe^{III}\text{-heme}]^+$ (quartet), and NO (doublet). The calculations were carried out using the Car−Parrinello molecular dynamics method,[35a] as implemented in the CPMD code.[35b,c] The Kohn−Sham orbitals are expanded in a plane wave (PW) basis set with the kinetic energy

(31) Ford, P. C.; Laverman, L. E. *Coord. Chem. Rev.* **2005**, *249*, 391.
(32) (a) Armentrout, P. B. *Annu. Rev. Phys. Chem.* **2001**, *52*, 423. (b) Rodgers, M. T.; Armentrout, P. B. *Acc. Chem. Res.* **2004**, *37*, 989. (c) Freiser, B. S. *Acc. Chem. Res.* **1994**, *27*, 353. (d) Bohme, D. K.; Schwarz, H. *Angew. Chem., Int. Ed.* **2005**, *44*, 2336. (e) Schroeder, D.; Schwarz, H. *Angew. Chem., Int. Ed.* **1995**, *34*, 1973. (f) Operti, L.; Rabezzana, R. *Mass Spectrom. Rev.* **2006**, *25*, 483. (g) Plattner, D. A. *Top. Curr. Chem.* **2003**, *225*, 153. (h) Gerdes, G.; Chen, P. *Organometallics* **2003**, *22*, 2217.
(33) Bartmess, J. E.; Georgiadis, R. M. *Vacuum* **1983**, *33*, 149.
(34) Anicich, V. A. *J. Phys. Chem. Ref. Data* **1993**, *22*, 1469.
(35) (a) Car, R.; Parrinello, M. *Phys. Rev. Lett.* **1985**, *55*, 2471. (b) *CPMD program*, Copyright IBM Corp. 1990−2003, Copyright MPI für Festkörperforschung, Stuttgart 1997−2001. URL: http://www.cpmd.org; (c) Marx, D.; Hutter, J. Ab Initio Molecular Dynamics: Theory and Implementation. In *Modern Methods and Algorithms of Quantum Chemistry*; Grotendorst, J., Ed.; John von Neumann Institute for Computing: Julich, Germany, 2000; p 301. (d) Carloni, P.; Rothlisberger, U.; Parrinello, M. *Acc. Chem. Res.* **2002**, *35*, 455.

cutoff of 70 Ry. Earlier calculations on iron-porphyrin models[21g,22b,23p] showed that this cutoff is sufficient for achieving a good convergence of energies and structural properties. The systems were enclosed in an orthorombic supercell of size 18 × 16.5 × 18 Å$^3$ periodically repeated in space. Ab initio pseudopotentials, generated within the Troullier−Martins scheme,[36] including the nonlinear core-correction[37] for the iron atom, were employed. Calculations were made using the generalized gradient-corrected approximation of the spin-dependent density functional theory (DFT-LSD), following the prescription of Becke and Perdew.[38] Structure optimizations were performed by means of molecular dynamics with annealing of the atomic velocities, using a time step of 0.072 fs and a value of 700 au for the fictitious electronic mass of the Car−Parrinello Lagrangian. Previous work has demonstrated the reliability of this computational setup in the description of structural, energetic and dynamical properties of heme-based systems.[21g,22b,23p] In particular, the structure and spin states of an iron-porphyrin were found to be in agreement with previous all-electron calculations[21l,m] as well as with more recent studies.[39] The performance of different exchange and correlation functionals in the modeling of heme systems was analyzed by Scherlis et al.[40] Structure analysis was performed with Visual Molecular Dynamics (VMD).[41]

**Acknowledgment.** This project was supported by the Italian Ministero dell'Università e della Ricerca, the Spanish Ministerio de Educación y Ciencia (Grant FIS2005-00655) and the Generalitat de Catalunya (Grant 2005SGR-00112). We acknowledge the computer support, technical expertise, and assistance provided by the Barcelona Supercomputing Center-Centro Nacional de Supercomputación (BSC-CNS).

**Supporting Information Available:** This material is available free of charge via the Internet at http://pubs.acs.org.

IC800953W

(36) Troullier, M.; Martins, J. L. *Phys. Rev. B* **1991**, *43*, 1993.
(37) Louie, S. G.; Froyen, S.; Cohen, M. L. *Phys. Rev. B* **1982**, *26*, 1738.
(38) (a) Becke, A. D. *J. Chem. Phys.* **1986**, *84*, 4524. (b) Perdew, J. P. *Phys. Rev. B* **1986**, *33*, 8822.
(39) Liao, M.-S.; Scheiner, S. *J. Chem. Phys.* **2002**, *116*, 3635.
(40) Scherlis, D. A.; Estrin, D. A. *Int. J. Quantum Chem.* **2001**, *87*, 158.
(41) Humphrey, W.; Dalke, A.; Schulten, K. *J. Mol. Graph.* **1996**, *14*, 33.